Journal of Sol-Gel Science and Technology (2021) 100:170–182
https://doi.org/10.1007/s10971-021-05627-6

ORIGINAL PAPER: SOL–GEL AND HYBRID MATERIALS WITH SURFACE MODIFICATION FOR APPLICATIONS

High-performance photocatalytic degradation of neutral red over cobalt grafted-mesoporous silica under UV irradiation

Fatemeh Mahfoozi[1] · Ali Mahmoudi[1] · Mohammad Reza Sazegar[1] · Khodadad Nazari[2]

Received: 24 March 2021 / Accepted: 16 August 2021 / Published online: 7 September 2021
© The Author(s), under exclusive licence to Springer Science+Business Media, LLC, part of Springer Nature 2021

Abstract

Cobalt-grafted-mesoporous silica nanoparticles with the Si/Co molar ratio of 70 were synthesized by using sol–gel method (denoted as Co-MSN). Characterization of the Co-MSN was carried out by X-ray diffraction analysis (XRD), Fourier-transform infrared spectroscopy (FTIR), energy dispersive X-ray analysis (EDX), scanning electron microscopy (SEM), and N_2 adsorption/desorption analysis. Photocatalytic activity of the Co-MSN sample was studied for removal of neutral red as one of the most widely used dye pollutants, in presence of H_2O_2 and UV irradiation. In this regard, effect of various influencing parameters such as pH, Co content, dye concentration, amount of oxidant, and presence/absence of UV irradiation were investigated. It was found that incorporation of the Co^{2+} ions into the mesoporous silica nanostructure significantly improves the photocatalytic degradation of neutral red. Under the optimized conditions including 0.3 mmol of H_2O_2 (as an oxidant), catalyst dosage of 0.075 mg, initial dye concentration of 0.08 mM, and UV irradiation (32 W, 254 nm), up to 81% of neutral red was degraded at room temperature for 220 min.

Graphical Abstract

The Co-MSN nanoparticles able to catalyze the photodegradation reaction of neutral red dye in the different H_2O_2 concentrations under UV irradiation with high performance, a green chemistry.

The Co-MSN nanoparticles able to catalyze the photodegradation reaction of Neutral Red dye in the different H_2O_2 concentrations under UV irradiation with high performance, a green chemistry.

Keywords Cobalt · Mesoporous silica · Photodegradation · Neutral red · H_2O_2 · Oxidation

1 Introduction

Every day, industrial effluents containing various pollutants, including paints, enter the surface, and groundwater resources. Dyes and pigments are widely used, mostly in food, paper, leather, plastics, textiles, and cosmetic industries. The release of dyestuff from these industries can lead to many environmental hazards. According to the Color Index (CI), more than 10,000 dyes are being used in various industries. For example, in China, large quantities of colored effluents (over 4.4×10^6 m^3 per day) with strong

✉ Ali Mahmoudi
mahmoudiali.ac@gmail.com

✉ Mohammad Reza Sazegar
m_r_sazegar@yahoo.com

[1] Faculty of Chemistry, North Tehran Branch, Islamic Azad University, Hakimiyeh, Tehran, Iran

[2] Future Bioenergy Solutions Inc., North Vancouver, BC V7P 3P9, Canada

persistent color and high biochemical oxygen demand are being discharged into the water resources, which are aesthetically and environmentally unacceptable [1]. Nowadays, many governments have imposed severe restrictions, and have forced dye-using industries to decolorize their effluents before discharge. Most of the dyes are toxic and must be removed before discharging into the streams since their effluents can reduce light penetration and photosynthesis. To date, various treatment technologies have been devised for dye removal. These may include activated sludge, chemical coagulation, and adsorption processes [2, 3].

Although adsorption founds superiority when some experimental parameters such as flexibility, simplicity, and ease of operation are considered [4, 5], certain limitations and drawbacks may restrict its application in large scale systems. For example, large amounts of adsorbents may lead to secondary environmental issues. In addition, recycling of some adsorbents may be very difficult or expensive. Getting rid of this type of waste, for example by incineration, may produce high amounts of pollutants, including greenhouse gases [6–8]. Although post-grafting with functional groups has been widely used to modify the porous structure of the silica-based mesoporous materials to get higher adsorption capacities, there are still major concerns about cost-effectiveness of some adsorbents such as carbon materials [9, 10].

Photodegradation is also a well known and widely used purification technique for the removal of certain pollutants from water, especially those which are practically unaffected by conventional wastewater treatments. Physicochemical processes such as photodegradation have also found their position in wastewater treatment. Combining UV irradiation and a typical oxidant such as hydrogen peroxide has been applied successfully in advanced oxidation processes (AOPs) to treat different pollutants in water [11–15]. Photodegradation has been described as the acceleration of a reaction under irradiation of either ultraviolet or visible light in the presence of a photocatalyst that can adsorb light to produce electron–hole pairs. Generation of free radicals in this process is responsible for the degradation of organic molecules to simpler species such as H_2O and CO_2 under mild conditions. This process has many advantages such as using low temperature, cost-effectiveness, and mild reaction conditions. Although nano-sized metal oxides have exhibited promising results as adsorbents in some water treatment processes, their roles as photocatalysts in photodegradation processes cannot be ignored [16–19].

Recently, application of the titanium dioxide to decorate natural cellulosic Juncus effusus fibers for highly efficient photodegradation of dyes is reported [4]. Moreover, reduced graphene oxide was synthesized and incorporated with zinc oxide nanomaterial to obtain a nanocomposite (ZnO/RGO), which shows up to 98% photocatalytic degradation of basic blue dye [20]. In another study, titanium oxide nanoparticles were doped with cobalt (denoted as Co/TiO_2) and used to photodegrade Amido Black dye in water, under UV radiation. The results showed a high-performance photodegradation of Amido Black, as high as 90%. The mechanism of this reaction was proposed to be based on the adsorption of Amido Black dye on the surface of cobalt-doped titanium oxide, followed by degradation under UV radiation [21]. Highly porous TiO_2-reduced graphene oxide (RGO) aerogel possessing high pore volume and large surface area was shown to have high photocatalytic efficiency in comparison with the TiO_2-graphene nanoparticles. The TiO_2-RGO aerogel photocatalyst exhibited excellent performance for dye photodegradation [22].

Dye photodegradation is a widely applicable technique to remove hazardous pollutants. However, most of the dyes such as neutral red have relatively high water solubility and this makes the conventional treatment methods ineffective for their removal from the wastewater. Neutral Red (Scheme 1) is a cationic dye that is used extensively for staining in histology. The dye's toxic nature can be easily understood by considering its materials safety data sheet. For example, its thermal decomposition causes hazardous products such as carbon monoxide (CO), carbon dioxide (CO_2), nitrogen oxides (NO_x), etc. Its other adverse effects may include carcinogenicity, high, and chronic toxicity [23].

Silica porous materials have been used as important nanocarriers for the photodegradation processes [24, 25]. Modification of the mesoporous silica nanostructures with transition metals such as Pt, Zr, Ni, Fe, Zn, and Co can considerably improve their photocatalytic activities [23, 26–32]. Among these metals, Co^{2+} ions can generate the electron (e−) and hole (h+) pairs, which in turn, can produce hydroxyl free radicals and superoxide anions. These species can degrade many organic molecules, including dyes, through a photocatalytic performance [21].

In this work, cobalt modified mesoporous silica nanoparticles (Co-MSN) with the Si/Co molar ratio of 70 were prepared by the sol–gel method. Here, for the first time, we used glycerol as a co-solvent in the synthesis of Co-MSN in comparison with the Co-MSN sample which has previously synthesized. Glycerol can better disperse the spherical mesoporous silica structure. Moreover, the hydrolysis

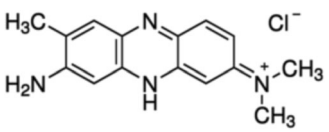

Scheme 1 Chemical structure of neutral red

reaction was carried out by ammonia 25% in this synthesis, while it was done previously by using sodium hydroxide.

Characterization of the catalyst was carried out by using X-ray diffraction analysis (XRD), Fourier-transform infrared spectroscopy (FTIR), energy dispersive X-ray analysis (EDX), BET, and scanning electron microscopy (SEM) techniques. The mesoporous silica nanomaterials are of great interest to researchers, and their metal-modified samples are applied as catalysts for the synthesis of many chemical compounds. The most common types of mesoporous nanoparticles are MCM-41 and SBA-15. The synthesis method and XRD analysis results were following the formation of the MCM-41 family structure for the Co-MSN. However, there were some differences with MCM-41 due to the cobalt grafting, which is reflected in the pore size and volume, and other related data that can be obtained from N_2-sorption isotherms.

The catalytic activity of this heterogeneous nanomaterial was investigated by studying the photocatalytic degradation of neutral red as a dye pollutant with a green chemistry approach. Effect of various parameters such as type and amount of oxidant, initial dye concentration, catalyst dosage, cobalt content, pH, and UV irradiation intensity was investigated to optimize the reaction conditions. Kinetic studies were also performed to determine the apparent k values, and the reaction intermediates were also identified. The current study provides a basis for the application of Co-MSN as a photocatalyst to alleviate the neutral red dye pollution. The novelty of this study included the high performance of the catalyst in Neutral Red decomposition in the neutral aqueous medium, the use of hydrogen peroxide as a mild oxidizer, the use of eco-friendly catalyst, and the easy workup of the catalyst.

2 Experimental

2.1 Materials and methods

Tetraethylorthosilicate (TEOS) was used as the silica source for the preparation of mesoporous silica nanoparticles (MSN). Cetyltrimethylammonium bromide (CTAB) was used as a template to direct the controlled synthesis of MSN. All of the chemicals, including $Co(NO_3)_2.6H_2O$ and neutral red, were purchased from Merck and used without further purification. A Millipore Milli-Q System was used to supply the required deionized water.

Powder X-ray diffraction (XRD) patterns were recorded on a Philips X-ray diffractometer (PW 1730) with automatic data acquisition (APD Philips v3.6B) at a scan rate of 0.1° 2θ/s, using Cu-Kα radiation (1.5406 Å). Cobalt content was determined by X-ray fluorescence spectrometry utilizing a Bruker S4 Explorer instrument equipped with a rhodium anode at 50 kV and 30 mA. Nitrogen adsorption/desorption isotherms were determined at 77 K on a BELSORP-MINI II instrument. Samples were degassed in vacuo and annealed at 250 °C for at least 6 h to remove moisture. Barrett–Joyner–Halenda (BJH) model was used for the evaluation of the pore size distribution. The morphology and particle size of the samples were determined by using a scanning electron microscope (SEM KYKY-EM-3200) with an accelerating voltage of 26 kV. Fourier-transform infrared (FTIR) spectra were recorded on a Rayleigh WQF-510 spectrophotometer using KBr disks. Ultraviolet–Visible (UV–vis) spectra of the dye solutions were recorded on a Varian, Cary 100 spectrophotometer using quartz cuvettes. UV irradiation was carried out by 4 × 8 W Siemens 4-pined single end UVC lamps (280 nm, maximum output at 254 nm).

2.2 Preparation of mesoporous silica nanoparticles (MSN)

MSN were synthesized according to the following method [33]. In a container, CTAB (3.7 g) was dissolved in deionized water (150 ml) at room temperature, followed by the addition of ethanol (absolute, 230 ml), and ammonia (25%, 14 ml). After stirring for 1 h, TEOS (15 ml) was added to the mixture for 5 h, and stirring was continued for 10 h. The white product was then aged for 24 h. After that, the precipitate was filtered and washed with a mixture of methanol and deionized water (1:5). The product was dried at 383 K overnight and then calcined at 823 K for 5 h to remove the remained organic materials.

2.3 Synthesis of Co-MSN

The cobalt-incorporated MSN was synthesized according to the following procedure. First, CTAB (3.7 g) was dissolved in deionized water (150 ml) at room temperature. Then an appropriate amount of $Co(NO_3)_2.6H_2O$ was added to obtain the desired Si/Co ratio (Si/Co = 70). The solution was placed in a water bath with 343 K. After stirring for about 30 min, ethanol (absolute, 230 ml), glycerol (20 ml, as a co-solvent), and ammonia (25%, 14 ml) were added in turn, and stirred at 343 K for 1 h. Then TEOS (15 ml) was added drop by drop to the mixture for 5 h and stirred at 343 K for 10 h. The white product was aged for 24 h. After this period of time, the results were filtered and washed twice (2 × 20 ml) with the solution of methanol and deionized water (1:5). To ensure the removal of any Co^{2+} ions adsorbed on the surface of the Co-MSN, the product was Soxhlet extracted with acetonitrile for 6 h before calcination. The precipitate was dried in an oven at 383 K for 20 h followed by calcination at 823 K for 3 h. finally, the obtained Co-MSN (1 g) was added to deionized water (50 ml) and stirred

Table 1 Description of the different reaction conditions as experimental codes M_1–M_{17}

Experiment code	Co-MSN (mg)	H_2O_2 Conc. (mM)	Dye Conc. (mM)	pH	UV Irradiation
M_1	0.05	0.1	0.08	7	✓
M_2	0.05	0.1	0.08	7	–
M_3	0.025	0.1	0.08	7	✓
M_4	0.025	0.1	0.08	7	–
M_5	0.025	0.5	0.08	7	✓
M_6	0.025	0.5	0.08	7	–
M_7	0.025	–	0.08	7	✓
M_8	0.025	–	0.08	7	–
M_9	–	–	0.08	7	✓
M_{10}	0.025	0.1	0.08	4	✓
M_{11}	0.025	0.1	0.08	9	✓
M_{12}	–	0.1	0.08	4	–
M_{13}	–	0.1	0.08	7	✓
M_{14}	–	0.1	0.08	7	–
M_{15}	MSN (0.025)	0.1	0.08	7	✓
M_{16}	MSN (0.025)	0.1	0.08	7	–
M_{17}	MSN (0.025)	–	0.08	7	–

Scheme 2 An illustration of the preparation of Co-MSN

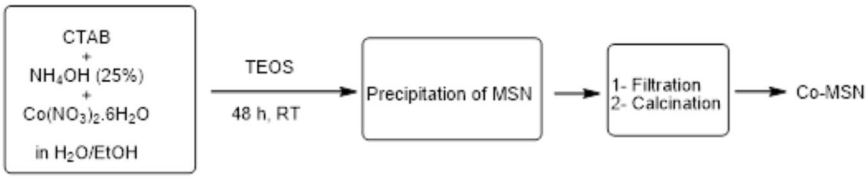

at room temperature for 3 h. The mixture was centrifuged at 4500 rpm for 20 min and the supernatant was tested by inductively coupled plasma (ICP) analysis to check the separated cobalt species from the Co-MSN framework.

2.4 Catalytic activity tests

The activity of the synthesized catalyst was studied for the degradation of neutral red dye in the presence of hydrogen peroxide solution at different acidities (pH = 4, 7, and 9), with or without UV irradiation at room temperature. The experiments were performed with two different Co-MSN loadings of 0.05 and 0.025 mg, and two concentrations of hydrogen peroxide (0.1 and 0.5 mM). In a typical procedure, the catalyst (3 mg) was sonicated in acetate buffer solution (2 ml, pH 4 or 7) for 20 min to prepare a stock dispersion. Then, neutral red dye (0.08 mM in acetate buffer), an appropriate amount of the Co-MSN stock dispersion (equivalent to 0.05 or 0.025 mg), and H_2O_2 (0.1 or 0.5 mM) were added to 2800 µl of acetate buffer and stirred under UV radiation (or without UV radiation) for 225 min. The trend of the neutral red degradation was monitored by UV–vis spectroscopy after filtration of the dispersed solid catalyst. The absorbance measurements were performed at λ_{max} of 520 nm [34]. The photo-reactor was made of an aluminum box with four UV lamps (8 W, Siemens, Germany) around the sample. Table 1 shows a list of the experimental parameters used in the photodegradation reactions.

3 Results and discussion

A schematic illustration of the preparation process of Co-MSN is presented in Scheme 2. The method of preparation is based on the hydrolysis of tetraethylorthosilicate in a basic medium. This hydrolysis reaction is an example of a sol–gel process. Although the side product of the reaction is ethanol, the TEOS itself should be dissolved in alcohol before hydrolysis.

3.1 Characterization of the catalysts

FTIR spectroscopy was used to investigate the presence of the expected functional groups in the MSN and Co-MSN samples. The results showed that the loading of cobalt in the pure MSN did not change the position of bands in the FTIR spectra, which indicates that the framework structure of MSN was not changed after cobalt modification.

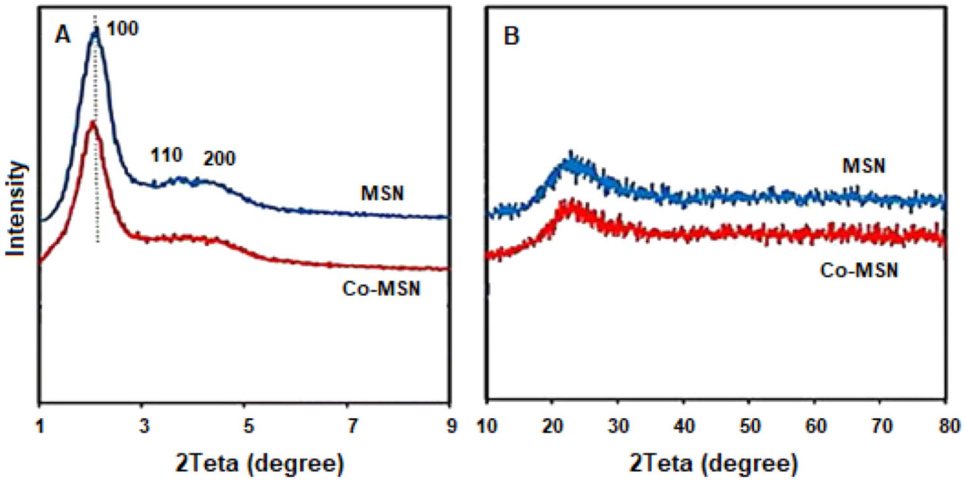

Fig. 1 XRD patterns of MSN and Co-MSN (**A**) low-angle and (**B**) high-angle

Table 2 Physicochemical properties of the synthesized MSN and Co-MSN samples

Catalyst	d_{100} (nm)	a_0 (nm)	S ($m^2\ g^{-1}$)	V_p ($cm^3\ g^{-1}$)	W (nm)	t (nm)	*Si/Co*
MSN	3.84	4.43	995	0.84	3.37	1.06	–
Co-MSN	3.90	4.68	691	0.70	3.20	1.48	70

d_{100} d-spacing of the plane direction (100) in Angstroms, a_0 pore center distance (equal to $2d_{100}/\sqrt{3}$, S surface area obtained from N_2 adsorption–desorption isotherms, V_p total pore volume, W pore size obtained from the BJH method, t pore wall thickness

The XRD pattern of the Co-MSN sample is compared with that of MSN in Fig. 1. Both are common in peaks at $2\theta = 2.4°$, 4.2°, and 4.7° in the low-angle pattern indexed to (100), (110), and (200) planes of two-dimensional hexagonal (p6mm) structure of mesoporous materials. It should be mentioned that the inclusion of cobalt resulted in some decrease of intensity of these peaks, along with a small shift of the most intense band to lower 2θ, which indicates some decrease in crystallinity of the structure due to replacement of Si by Co, along with increased d_{100}-spacing. The XRD pattern of Co-MSN can show the presence of cobalt oxide in the nanoparticles. Since the higher ionic radius of Co (II), the change in d_{100} spacing in the plane of Co-MSN clearly can be indicated by the incorporating of cobalt atoms in the MSN framework. Therefore, this is a direct indication of the replacement of some Si (IV) ions with Co (II) species.

The formation of the Co–O–Si bond has been suggested as a justification for the observed shift in the peak positions [31]. In the high-angle patterns, on the other hand, a broad peak was observed around 22°, which originates from amorphous silica [35].

Table 2 shows the physicochemical properties of MSN and Co-MSN samples based on the results of the BET analysis. It is clear that after the incorporation of cobalt, the total pore volume and the BET surface area was decreased [32]. It is also noteworthy that an increase in the wall thickness after incorporation of cobalt is in line with increased d_{100}-spacing, as concluded by the XRD analysis.

Figure 2 exhibits the N_2 adsorption–desorption isotherms for the MSN and Co-MSN samples. Both samples exhibited a type (IV) isotherm with H4-type hysteresis loops in the P/P_0 range of 0.3–0.8, which is characteristic of well-ordered mesoporous materials. The corresponding pore diameters were 3.37 and 3.2 nm for the MSN and Co-MSN samples, respectively (Table 2). The increased adsorbed volume at higher P/P_0 values may be an indication of a secondary mesoporous system with slit-like pores.

Figure 3 shows the UV–vis DR spectra of the MSN and Co-MSN catalysts. The presence of three peaks at the regions of 535, 585, and 650 nm for the cobalt-containing MSN are indicated to the Jahn–Teller distortions or spin–orbit coupling during $^4A_2(F) \rightarrow {}^4T_1(P)$ transition and shows the cobalt atoms are located in tetrahedral coordination into the MSN framework [31].

Figure 4A, B shows the SEM images of MSN and Co-MSN samples. They exhibit spherical shapes with an average particle size of 100–300 nm. To confirm the presence of cobalt in the Co-MSN sample, energy dispersive X-Ray analysis (EDS) was performed and the result is presented in Fig. 4C. All of the anticipated K and L lines of Co, O, and Si were observed at estimated positions. Figure 4D exhibits a photo of the Co-MSN sample. All of these results are in agreement with our previous findings on the presence of Co^{2+} in the framework of MSN as building blocks instead of being adsorbed or charge compensating species [27, 32–37].

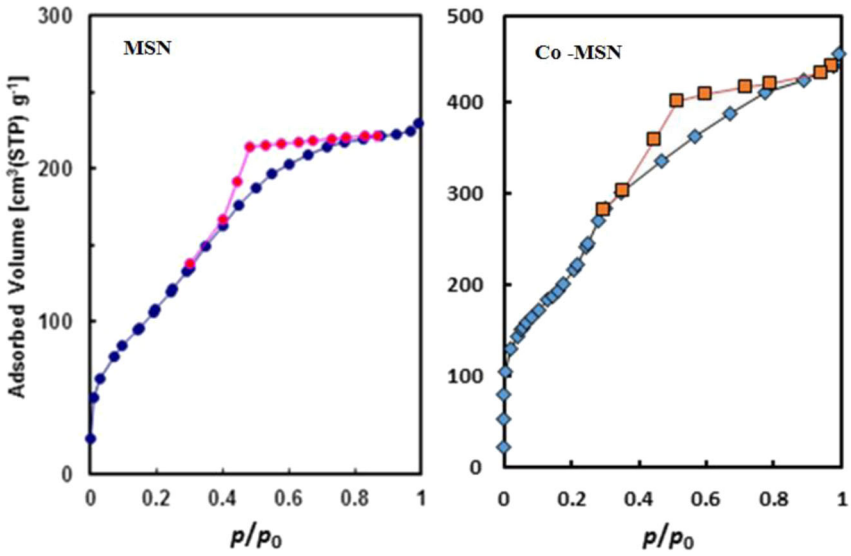

Fig. 2 N_2 adsorption–desorption isotherms for the MSN and Co-MSN samples

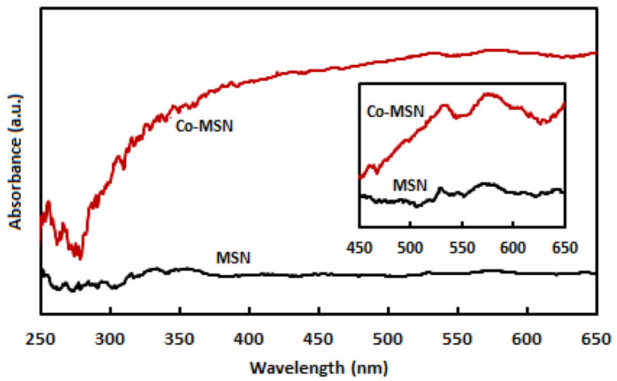

Fig. 3 Diffuse reflectance spectra of the Co-MSN samples

It should also be noted that soxhlet extraction of the Co-MSN sample with acetonitrile before calcination, rejected the presence of any surface Co^{2+} ions. The soxhlet extraction with a coordinating solvent such as MeCN has been reported as an effective method for the probable removal of the surface adsorbed ions in many papers, especially after ion-exchange processes [38–40]. However, our UV–vis analysis did not show any trace of Co (II) in the extraction solvent after 6 h. ICP analysis was carried out for the Co-MSN sample after washing with an aqueous solution and showed there were not any cobalt species in the aqueous solution.

3.2 Photocatalytic activity for neutral red

To study the photocatalytic degradation of neutral red, the effect of various parameters such as UV irradiation, pH, Co content, dye concentration, and amount of oxidant was investigated. According to the obtained results, the photocatalytic degradation of neutral red was more effective under UV radiation than in the dark or under visible light. Figure 5 exhibited a trend of degradation of neutral red by MSN with/without UV irradiation, and also the effect of UV light intensity on photodegradation of neutral red dye.

In addition, in Fig. 5A one can note that some dye removal has occurred at the initial stage of the process. This may be due to the adsorption of the dye molecules by the mesoporous structure. at the beginning of the reaction (time = 0) when bare MSN was used without the oxidant and UV irradiation, about 18% of dye was removed after the end was removal 25% (time = 220 min) and when bare MSN was used without UV irradiation, about 34% of dye was removed this was enhanced to 40.5% when both UV and oxidant were used (Table 1, entries M_{15}, M_{16}, and M_{17}). shows that the percentage of dye removal which reveals higher in the presence of UV irradiation at the entire reaction time, thus M_{15} shows more activity in dye degradation in comparison with M_{16} and M_{17}. The effect of UV light intensity on the degradation of neutral red was also studied and the results are depicted in Fig. 5B. The results show that irradiation at 16 W had not a significant effect on the photodegradation process and the degradation efficiency was almost similar to that obtained without UV light. Increasing the light intensity from 16 to 32 W, however, resulted in higher efficiency. This enhancement may be due to the increase in the formation of $OH^{\bullet}$ concentration. The rate of photolysis of H_2O_2 depends directly on the irradiated light intensity. It is well known that at the low UV intensities, the rate of photolysis of H_2O_2 is limited and at high power, more hydroxyl radicals are formed due to photodissociation of H_2O_2 [36, 37].

Most of these studies have shown that the effect of H_2O_2 is related to many parameters including the H_2O_2 concentration, irradiation intensity, pH of the solution, and

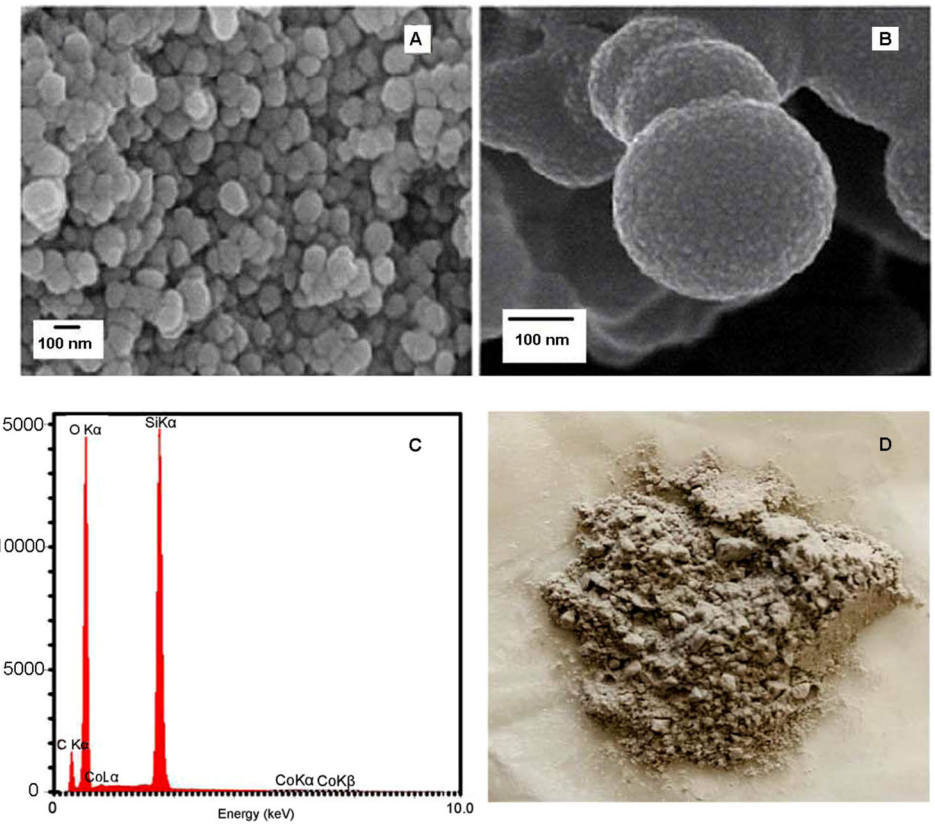

Fig. 4 SEM images of (**A**) MSN, (**B**) Co-MSN, (**C**) EDS analysis of Co-MSN, and (**D**) optical image of Co-MSN

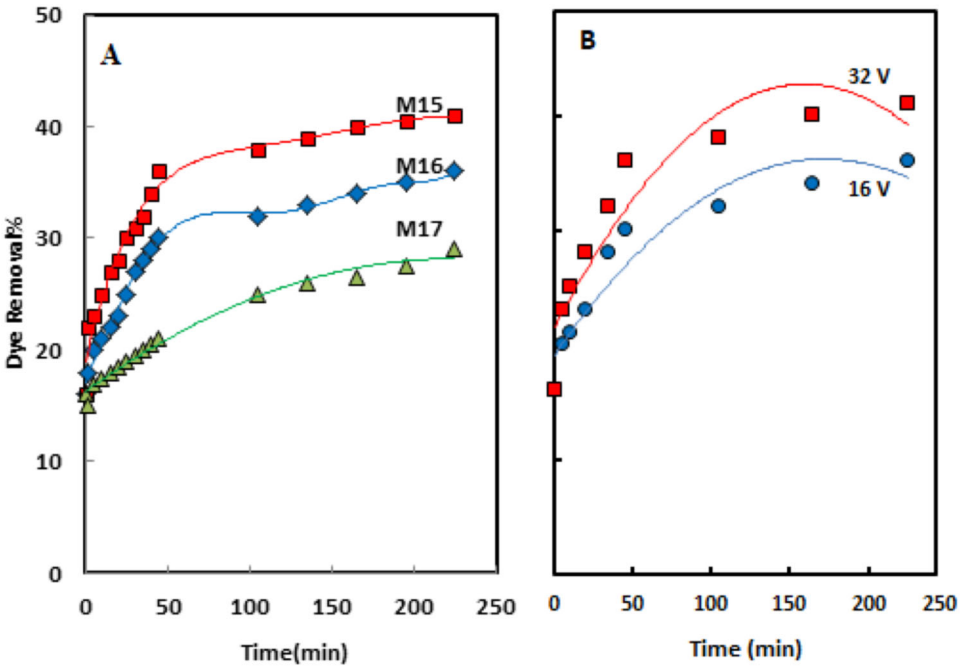

Fig. 5 (**A**) Trend of degradation of neutral red by MSN in the presence and absence of UV irradiation, and (**B**) effect of UV light intensity on photodegradation of neutral red

characteristics of the photocatalyst [41]. Galindo and Kalt [3] demonstrated that the UV/H_2O_2 combination can destroy the chromophore structure of azo dyes, and the reaction rate depends on the chemical structure and auxiliary groups attached to the aromatic nuclei of the dye molecules. Colonna et al. reported that UV irradiation in the presence of H_2O_2 leads to complete decolorization and mineralization of sulfonated azo and anthraquinone dyes [15]. The mechanism of dye destruction in the AOPs is based on the formation of very reactive hydroxyl radicals

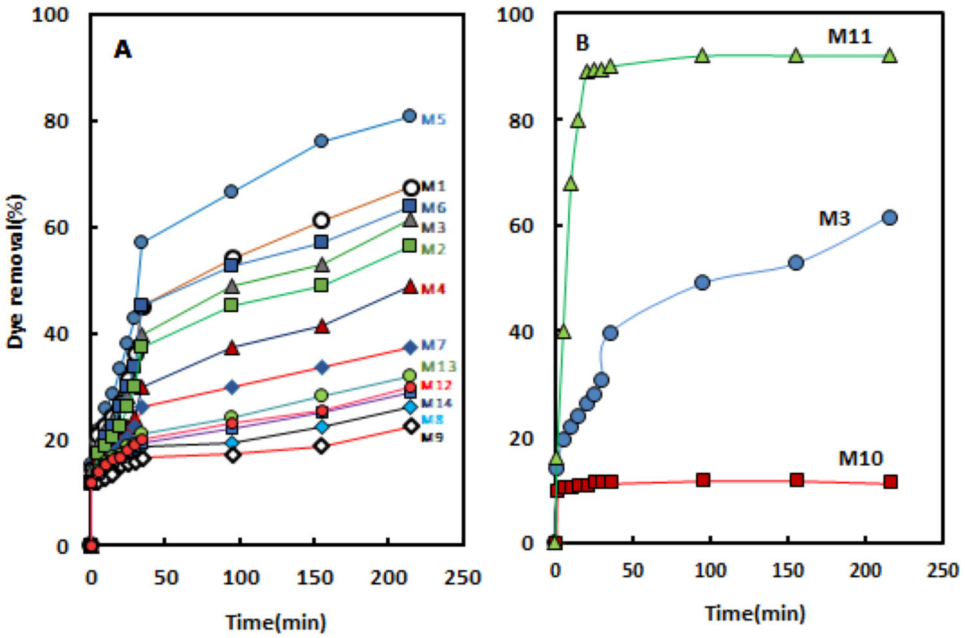

Fig. 6 (**A**) Effect of H_2O_2 and Co-MSN concentrations in neutral red photodegradation with/without UV light; (**B**) effect of pH (4, 7, 9) in neutral red photodegradation with $[H_2O_2] = 0.1$ mM and [Co-MSN] = 0.025 mg under UV irradiation

with an oxidation potential of 2.80 V, which may result in the oxidation of a broad range of organic compounds [42, 43]. Furthermore, an additional advantage of the UV/H_2O_2 process is the prevention of sludge formation during the different stages of the treatment. It can be carried out under ambient conditions and may lead to the complete mineralization of organic carbon into CO_2 [44]. Further optimization for taking into account the role of pH showed that the degradation reaction was pH-dependent. The efficiency of H_2O_2 in the absence of both catalyst and UV irradiation was studied on the neutral red photodegradation that good results were obtained at pH = 7. The presence of both catalyst and UV irradiation drastically increased the efficiency. Although the high pH is in favor of the formation of hydroxyl radicals, the presence of a metal such as cobalt will increase their aggressive nature. The effect of the pH on the degradation of neutral red is shown in Fig. 6B. Increasing the pH of the solution from 4.0 to 9.0 significantly can increase the dye removal efficiency in the presence of the Co-MSN catalyst, H_2O_2, and UV irradiation. Despite the best result was obtained at pH 9.0, the outstanding of this study is obtain a high-performance degradation at pH = 7. Higher amounts of the oxidant, on the other hand, resulted in an increase in dye removal. Nevertheless, taking into account the principles of green chemistry, efforts were made to use less oxidant. This was achieved when Co-MSN was used instead of MSN.

The results of these unique conditions were only the low degree of neutral red photodegradation. While in experiments involving all three factors of UV irradiation, hydrogen peroxide, and the Co-MSN catalyst, the rate of photodegradation has increased dramatically. The samples of M_1–M_{12} were listed in Table 1 and showed the conditions and results of these nanomaterials. The samples of M_8, M_9, and M_{12} are related to the use of the Co-MSN, UV irradiation, and H_2O_2 alone, respectively. The results exhibited the activity of 24%, 21.5%, and 26% for M_8, M_9, and M_{12}, respectively.

3.3 Proposed mechanism for the photodegradation reaction

The rate of photochemical degradation by H_2O_2 depends on the pH value, and this can provide a platform for the UV/H_2O_2 reaction to degrade different contaminants [43–45]. In the UV irradiation/H_2O_2 system, the addition of hydrogen peroxide and UV irradiation may facilitate the production of radicals that degrade complex organic contaminants into smaller molecules, hence further reduced the effluent color. Variations of UV irradiation with and without hydrogen peroxide addition were applied and the hydrogen peroxide concentration of 0.1 mM was chosen as the optimum dose.

At high pH values, hydrogen peroxide deprotonates to form an H_2O_2/HO_2^- equilibrium. The HO_2^- species react with H_2O_2 according to the following equation, to form molecular oxygen and water, instead of producing hydroxyl radicals under UV irradiation. Therefore, the instantaneous concentration of $OH^\bullet$ is lower than expected:

$$HO_2^- + H_2O_2 \rightarrow H_2O + O_2 + OH^- \quad (1)$$

Furthermore, the deactivation of $OH^\bullet$ is more important at high pH. The reaction of $OH^\bullet$ with HO_2^- is approximately 100 times faster than its reaction with H_2O_2. Also, at high pH, the H_2O_2 becomes highly unstable and undergoes

self-decomposition [46, 47]. The self-decomposition will rapidly break down the H_2O_2 molecules into water and oxygen as follows:

$$2H_2O_2 \rightarrow 2H_2O + O_2 \quad (2)$$

However, the better performance of the catalyst at high pH can be related to its structure. It is well known that the surface of silica materials is generally covered by silanol groups. These –OH functionalities can be used, for example, in surface modification reactions. At high pH, the neutral red is present as a free base rather than its hydrochloride form, and this brings the molecule to the positively charged surface of the catalyst, where it can react with the oxidant. Although the obtained results indicated that the alkali pH showed better dye degradation in comparison to the neutral and acidic media, because of economic and green chemistry considerations, this pH is not suitable for dye removal due to the harmful effects of alkali pH on the environment. Therefore, the photodegradation was carried out in a neutral medium. Thus this reaction occurred by using the Co-MSN in the pH = 7 with 0.025 concentration and $[H_2O_2] = 0.1$ mM.

To measure the charges of these nanomaterials, zeta (ζ) potential measurement was performed that showed −16.5 mV for MSN and +8.12 mV for the Co-MSN catalyst.

Figure 6A shows the effect of H_2O_2 and Co-MSN concentrations in the photodegradation of neutral red with/without UV irradiation, and Fig. 6B illustrates the effect of three different pH of 4,7, and 9 in neutral red photodegradation with the constant H_2O_2 concentration of 0.1 mM and Co-MSN concentration of 0.025 mg under UV irradiation. The results showed that the degradation efficiency over Co-MSN was increased when a combination of UV irradiation and an oxidant was used. It should be noted that in the absence of the Co-MSN catalyst and the presence of 0.1 mM H_2O_2 at pH 7, at the beginning of reaction the degradation efficiency showed only 18% (time = 0) then in presence of 0.1 mM H_2O_2 was 25%,(time = 220 min), (Table 1, the sample of M_{14}). This efficiency was increased to 30% upon irradiation of UV light(time = 220 min) (Table 1, the samples of M_{13}).

An increase in the H_2O_2 concentration from 0.1 mM to 0.5 mM resulted in an enhancement in the degradation efficiency under UV radiation from 75% to 81%, respectively (Fig. 6A). This enhancement may be associated with several factors related to the presence of H_2O_2. Hydrogen peroxide can produce hydroxyl radicals and accelerate the photocatalytic processes [38]. Hydroxyl radicals may be generated by direct photolysis of hydrogen peroxide [39, 40], or by the reaction of hydrogen peroxide with the superoxide radicals [41, 48, 49]. It has been shown that the initial amount of H_2O_2 affects the efficiency of the catalyst [50]. The effect of hydrogen peroxide on the photodegradation of organic contaminants in water, and inspecting its optimum concentration has been the subject of many studies [41, 51–53].

The results of this reaction showed that increasing the catalyst did not cause a significant increase in photodegradation efficiency in the presence of UV irradiation. It should be mentioned that higher amounts of the catalyst have been affected the yield considerably. hence 0.025 mg of the catalyst 0.08 mM of neutral red and concentrations 0.1 mM of hydrogen peroxide and pH = 7 were studied as the preferred media.

A kinetic study of the photodegradation of Neutral Red was also performed to get an insight into the reaction mechanism. The kinetic study was undertaken by using the Langmuir–Hinshelwood kinetics model. It was found that degradation of neutral red follows a pseudo-first-order kinetic with the apparent rate constant being calculated as $\ln C/C_0 = k_{app}t$, where C_0 is the initial concentration and C is the residual concentration of the Neutral Red at the exposure time t, measured at room temperature in pH = 7. The value of k for the optimized reaction conditions was found to be 220 min^{-1} (Fig. 7A). To compare the effect of the various reaction conditions on the kinetics of the neutral red degradation, the plot of the $\ln C/C_0$ vs. time is presented for the M1–M4 in Fig. 7B.

According to the data in Table 1 and Figs. 6, 7B, a combination of the UV irradiation, H_2O_2, and Co-MSN can be degraded the neutral red efficiently (M_1 and M_3). The significant photodegradation rate enhancement from M_4 to M_1 (0.25 to 0.35 min^{-1}) is about 73%, which is thought-provoking. Therefore, the use of the Co-MSN catalyst, UV irradiation, and peroxide, showed a synergistic effect on both of the rate and efficiency of the photocatalytic dye degradation.

Generally, it is believed that radical photooxidation of dyes concerning dye concentration follows a pseudo-first-order mechanism. Based on the obtained results and published literature [35], the following mechanistic pathway may be involved in the photodegradation of neutral red (Eqs. 3–6):

$$Co + h\upsilon \rightarrow e_{cb}^- + h_{vb}^+ \quad (3)$$

$$H_2O + h_{vb}^+ \rightarrow OH^\bullet + H^+ \quad (4)$$

$$H_2O_2 \rightarrow 2\,OH^\bullet \quad (5)$$

$$OH^\bullet + \text{Neutral Red} \rightarrow \text{Mineralization products} \quad (6)$$

Where e_{cb}^- and h_{vb}^+ refer to the electron in the conductive band, and the hole in the valence band of the photocatalyst, respectively. The proposed mechanistic pathway may be illustrated as follows:

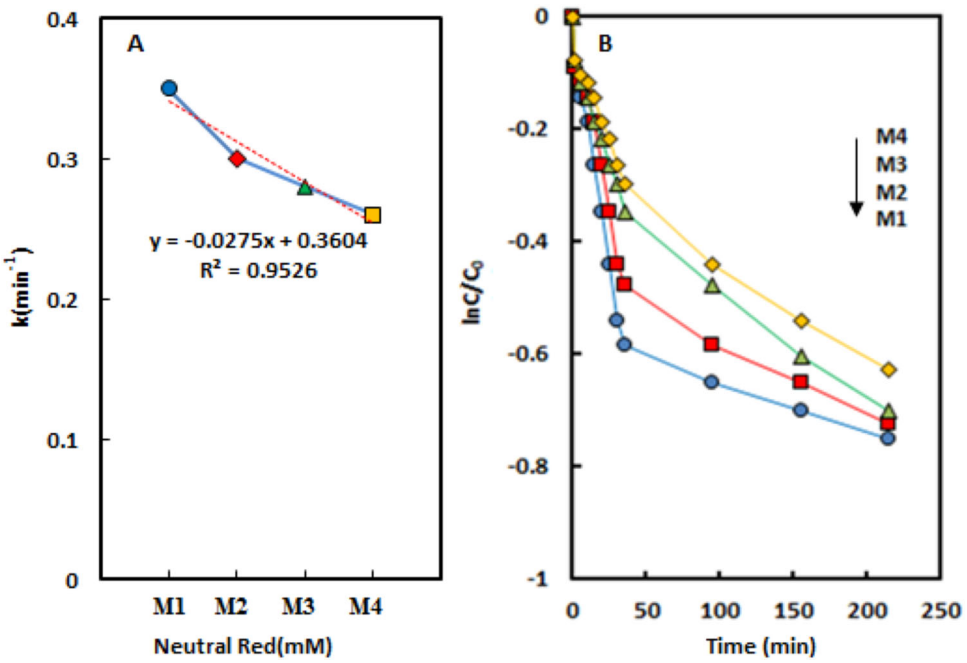

Fig. 7 **A** Pseudo-first-order k_{app} constants under different conditions, and (**B**) plot of lnC/C_0 vs. time for photodegradation of neutral red for the catalysts of M_1–M_4

Table 3 A comparison of the cobalt-mediated methods for the photocatalytic degradation of neutral red

Photocatalyst	Synthesis method	Neutral red conc. (mg)	Catalyst amount (mg)	Time (min)	Temp. (°C)	pH	Efficiency (%)	Ref.
Co-MSN	Sol–gel	23	0.025	225	23	7	81	This work
$Co_4[Fe(CN)_6]$	Chemical precipitation	17	175	120	–	–	68	[56]
(MFe_2O_4: M = Co, Ni, Cu, Zn)	–	10	0.5	300	–	7	60	[57]
Co_2SnO_4	–	10	0.5	240	25	5	85	[58]
GNs/Co-Mn	Chemical reduction	5	20	30	25	7	94	[59]
Cobalt(II) hexacyanoferrate	Hydrothermal	17	150	120	25	5	80	[60]
$LaCoO_3$	Surface ion adsorption	10	200	100	25	7	90	[61]

According to the suggested mechanism, UV irradiation produces a hole in the valence band of the photocatalyst, which can oxidize a water molecule to hydroxyl radicals. These radicals can produce further hydroxyl radicals from the hydrogen peroxide molecules. Hydroxyl radicals are generally aggressive species that can mineralize most of the organic molecules, including dyes. To approve the suggested mechanism, the addition of a radical scavenger was tested. It was observed that the photodegradation of neutral red was stopped after adding 2-propanol to the reaction mixture which indicated the involving a radical mechanistic pathway [54, 55]. Therefore, it can be concluded that the cobalt-mediated generation of hydroxyl radicals is responsible for this type of photodegradation (Eq. 7):

$$(CH_3)_2CHOH + O \rightarrow (CH_3)_2O + H_2O \quad (7)$$

To highlight the advantages of the present study, a comparison was made between the Co-MSN catalyst and the reported cobalt-containing catalysts for the degradation of neutral red. The results are summarized in Table 3 and indicate the relative advantages of the Co-MSN for the degradation of neutral red. High efficiency of dye degradation was observed in the presence of less amount of the catalyst Co-MSN (0.025 mg) at neutral pH than the higher amount of the other catalysts (0.5, 20, 150, 175, and 200 mg) [56–61]. This indicating the outstanding higher activity of the Co-MSN catalyst in comparison to the other catalysts for dye photodegradation Scheme 3.

3.4 Recyclability of the catalyst

To evaluate the recyclability of the photocatalyst, its usage in multiple reaction runs was studied. To do so, after the completion of each reaction, the reaction mixture was centrifuged and the precipitates were rinsed with methanol (3 × 10 mL) and dried at 110 °C for 4 h, then it was reused

Scheme 3 A proposed mechanistic pathway for photodegradation of neutral red by Co-MSN

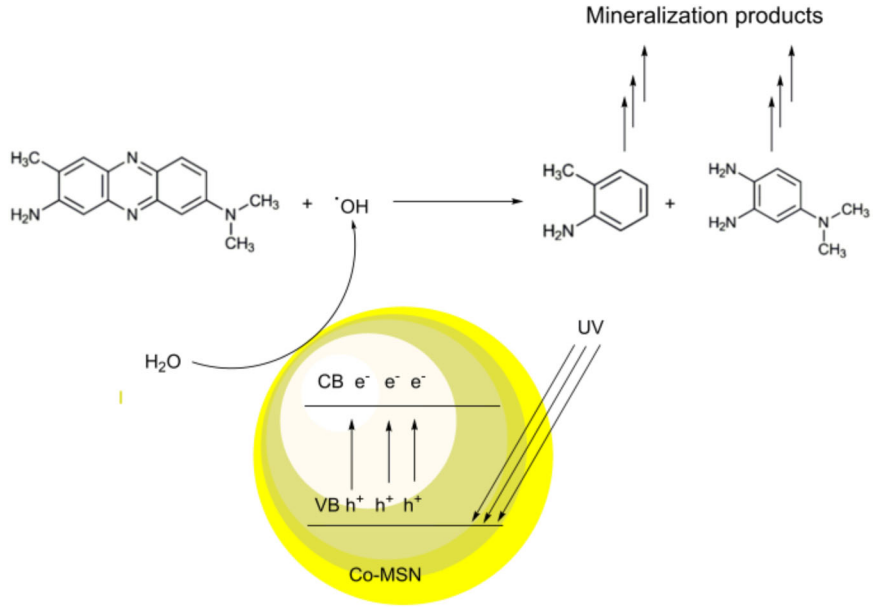

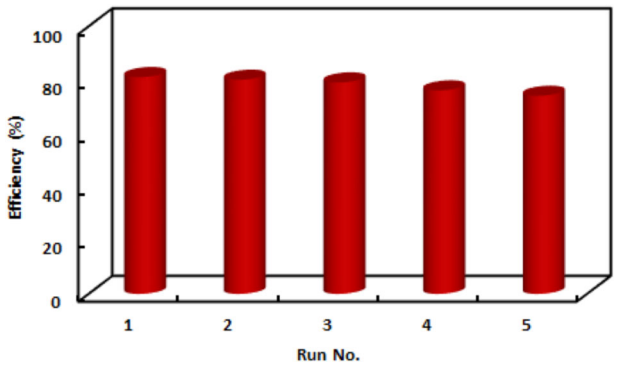

Fig. 8 Recyclability of the Co-MSN during five runs

in the next reaction run. Figure 8 presents the results of five successive runs. As it is clear, only a 7 percent loss of activity was observed (81% yield for the first run to 74% yield for the fifth run), which indicated a bit of deactivation in the solid catalyst.

To investigate the structural changes of the catalyst during the reaction, the recycled catalyst of the final run was characterized using XRD patterns, SEM imaging, EDX, and FTIR spectroscopy. Figure 9 exhibits the crystal structure (Fig. 9A), morphology (Fig. 9B), and functional groups (Fig. 9C) of the catalyst before and after the photodegradation process. The results illustrated that the XRD patterns, morphology, and presence of the functionalized groups of the Co-MSN catalyst were not considerably altered during the reaction. This indicates that the catalyst is robust enough to tolerate the harsh photodegradation conditions. In addition, EDX analysis showed exactly the presence of cobalt species in the before and after five recycling reactions (Fig. 9D). These results indicated the presence of cobalt species in the modified MSN structure.

Figure 10a depicts the trend of neutral red color change by photodegradation process within 220 min and Fig. 10b shows the UV spectra of the starting materials and the final products which have been monitored by UV–vis spectrophotometer.

Compared to the other studies (Table 3), following the green chemistry strategy, the new findings of photocatalytic degradation process using the Co-MSN catalyst including, high-performance photodegradation in neutral media, no further sludge or secondary waste generation, and less operational cost. For an industrially important process, it is vital to consider the role of the environment. This research is a preliminary study to evaluate the potential of the synthesized catalyst as a photocatalyst. Moreover, the use of environmentally friendly chemicals in a chemical process in green chemistry reactions is essential. Neutral red dye is used as a colorant in clinical laboratories to calculate chromogenic materials.

4 Conclusion

The modified MSN with Si/Co molar ratio of 70 (Co-MSN) were synthesized and characterized. The photocatalytic activity of the obtained product was compared with MSN nanoparticles in the photocatalytic degradation of neutral red as a representative dye. Effect of various parameters such as pH, dye and catalyst concentration, amount of oxidant, and presence/absence of UV irradiation was investigated. It was found that UV irradiation considerably improves the degradation yield and the best results were obtained by using an array of 4 × 8 W (254 nm) UV lamps. Further improvement was achieved when hydrogen

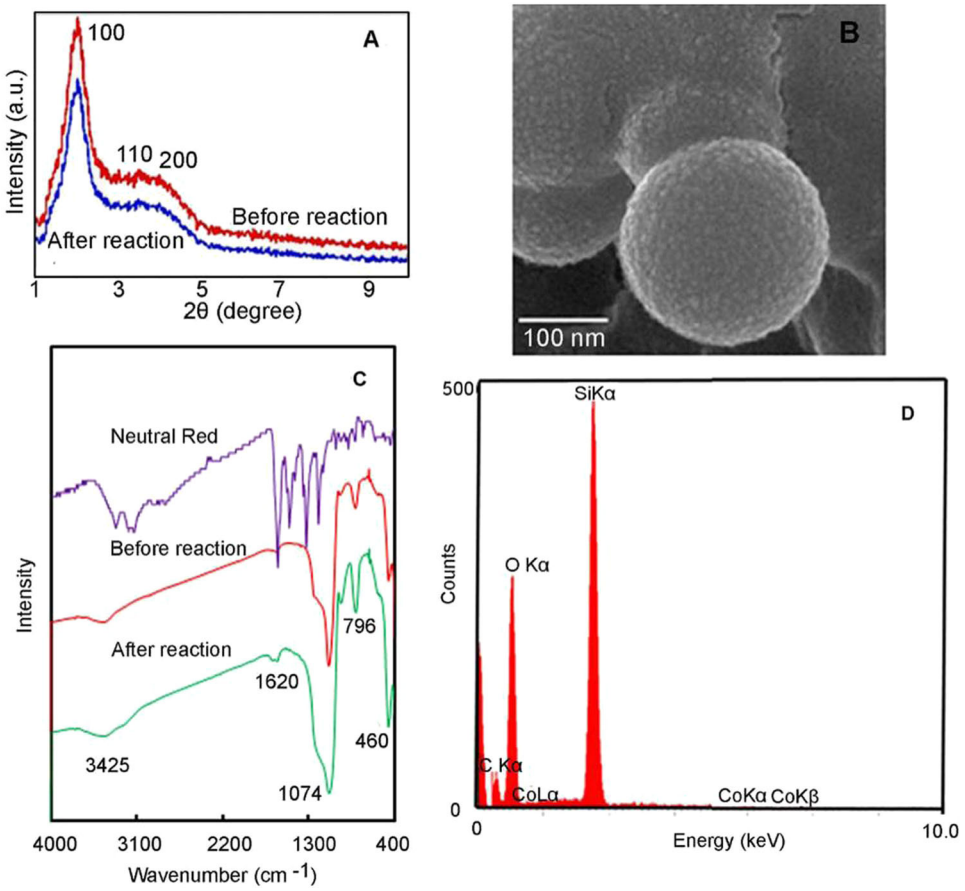

Fig. 9 (**A**) XRD patterns, (**B**) SEM image, and (**C**) FTIR spectra of the Co-MSN catalyst before and after photocatalytic reaction, (**D**) EDX analysis of the recycled Co-MSN

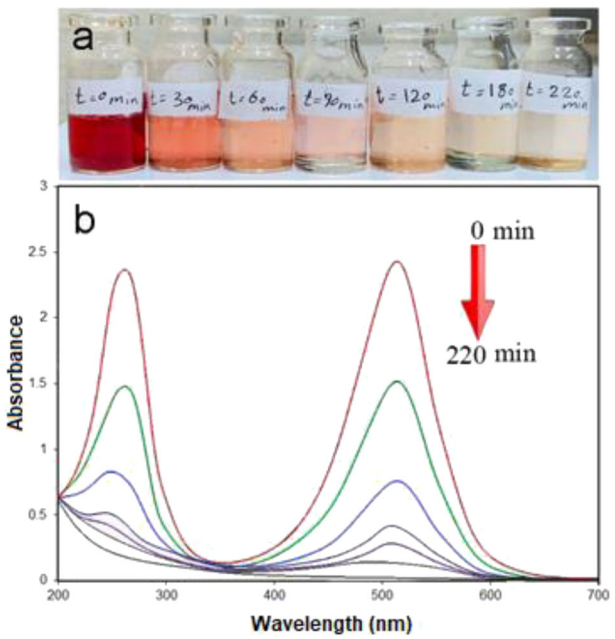

Fig. 10 The trend of color change (**a**) along with the corresponding changes in the UV–vis spectrum (**b**) of neutral red within 220 min

peroxide was used as an oxidant agent. Although at pH = 9 the degradation process was performed more readily, from green chemistry and economy point of view, the pH = 7 was selected as a preferred acidity. Under the optimized conditions, up to 81% of neutral red was degraded after 220 min. in the presence of Co-MSN.

A comparison between Co-MSN and the other cobalt-containing catalysts for the neutral red photodegradation process clearly showed the high power of this catalyst with a less amount of used catalyst.

The significant advantages of using the Co-MSN catalyst for the photodegradation of neutral red include a green chemistry approach, high efficiency in pH = 7, lack of formation of sludge and other waste material, and less cost of the catalyst and degradation process.

Acknowledgements We thank the deputy of the research center, Islamic Azad University, Tehran North Branch for helping with this study.

Compliance with ethical standards

Conflict of interest The authors declare no competing interests.

Publisher's note Springer Nature remains neutral with regard to jurisdictional claims in published maps and institutional affiliations.

References

1. Hickman R, Walker E, Chowdhury S (2018) J Water Process Eng 24:74
2. Mallakpour S, Rashidimoghadam S (2019) In: Deorge Z (ed) Composite Nanoadsorbents, 1st edn, Elsevier, p. 211–243.
3. Yan Y, Yang H, Yi Z, Xian T, Wang X (2019) Environ Sci Pollut Res Int 26:29020
4. Zhou S, Xia L, Zhang K, Fu Z, Wang Y, Zhang Q, Zhai L, Mao Y, Xu W (2020) Carbohydr Polym 232:115830
5. Assis Filho RBD., Araújo CMBD, Baptisttella AMS, Batista EB, Barata RA, Ghislandi MG, Motta Sobrinho MAD (2019) Environ Technol 1
6. Lin Y, Fang G, Deng Y, Shen K, Huang C, Wu T (2019) BioResources 14:5573
7. Novais RM, Carvalheiras J, Tobaldi DM, Seabra MP, Pullar RC, Labrincha JA (2019) J Clean Prod 207:350
8. Seidmohammadi A, Asgari G, Dargahi A, Leili M, Vaziri Y, Hayati B, Shekarchi A, Mobarakian A, Bagheri A, Nazari Khanghah S (2019) Prog Color Color Coat 12:133
9. Wu FC, Tseng RL, Juang RS (2005) J Colloid Interface Sci 283:49
10. Wu CH, Hazard J (2007) Mater 144:93
11. Li Y, Li L, Chen ZX, Zhang J, Gong L, Wang YX, Zhao HQ, Mu Y (2018) Chemosphere 192:372
12. Yu X, Lin X, Feng W, Li W (2019) Appl Surf Sci 465:223
13. Morrison C, Bandara J, Kiwi J (1996) J Adv Oxid Technol 1:160
14. Abdulhameed AS, Mohammad AT, Jawad AH (2019) J Clean Prod 232:43
15. Colonna GM, Caronna T, Marcandalli B (1999) Dyes pigm 41: 211
16. Pirillo S, Ferreira ML, Rueda EH (2009) J Hazard Mater 168:168
17. Sanchez LM, Ollier RP, Gonzalez JS, Alvarez VA (2018) In: Hussain CM (ed) Handbook of nanomaterials for industrial applications, Elsevier, p. 922–951
18. Adeleye AS, Conway JR, Garner K, Huang Y, Su Y, Keller AA (2016) Chem Eng J 286:640
19. Afkhami A, Moosavi R (2010) J Hazard Mater 174:398
20. Aqad KMA, Basheer C (2021) J Phys Org Chem 34:e411. https://doi.org/10.1002/poc.4117
21. Ali Imran, Alharbi OmarML, Alothman ZeidA, Badjah AY (2018) Photochem Photobiol 94:935
22. Sun X, Ji S, Wang M, Dou J, Yang Z, Qiu H, Kou S, Ji Y, Wang H (2020) J Alloy Compd 819:153033
23. Jamshidi D, Sazegar MR (2020) Int J Nanomed 15:871
24. Hua M, Zhang S, Pan B, Zhang W, Lv L, Zhang Q (2012) J Hazard Mater 211:317
25. Khajeh M, Laurent S, Dastafkan K (2013) Chem Rev 113:7728
26. Zhu J, Wang T, Xu X, Xiao P, Li J (2013) Appl Catal B-Environ 130:197
27. Sazegar MR, Dadvand A, Mahmoudi A (2017) RSC Adv 7:27506
28. Liang C, Niu C-G, Zhang L, Wen X-J, Yang S-F, Guo H, Zeng G-M (2019) J Hazard Mater 361:245
29. Valles VA, Sa-ngasaeng Y, Martínez ML, Jongpatiwut S, Beltramone AR (2019) Fuel 240:138
30. Choopan Tayefe H, Sazegar MR, Mahmoudi A, Jadidi K (2019) J Nanostruct 9:712
31. Hajiagha NG, Mahmoudi A, Sazegar MR, Pouramini MM (2019) Microporous Mesoporous Mater 274:43
32. Tayefe HC, Sazegar MR, Mahmoudi A, Jadidi K (2021) Silicon 13:677
33. Sazegar MR, Jalil AA, Triwahyono S, Mukti RR, Aziz M, Aziz MAA, Kamarudin NHN, Setiabudi HD (2014) Chem Eng J 240:352
34. Kumari S, Dhar BB, Panda C, Meena A, Sen Gupta S (2014) ACS Appl Mater Interfaces 6:13866
35. Kamarudin NHN, Jalil AA, Triwahyono S, Artika V, Salleh NFM, Karim AH, Jaafar NF, Sazegar MR, Mukti RR, Hameed BH, Johari A (2014)J Colloid Interface Sci 421:6
36. Kamarudin NHN, Jalil AA, Triwahyono S, Sazegar MR, Hamdan S, Baba S, Ahmad A (2015) RSC Adv 5:30023
37. Aghayan M, Mahmoudi A, Nazari K, Dehghanpour S, Sohrabi S, Sazegar MR, Tabrizi NM (2019) J Porous Mater 26:1507
38. Alnuaimi MM, Rauf M, Ashraf SS (2008) Dyes Pigm 76:332
39. Binas V, Venieri D, Kotzias D, Kiriakidis G (2017) J Materiomics 3:3
40. Ollis DF, Pelizzetti E, Serpone N (1991) Environ Sci Technol 25:1522
41. Poulios I, Micropoulou E, Panou R, Kostopoulou E (2003) Appl Catal B-Environ 41:345
42. Furatian L, Mohseni M (2018) J Photochem Photobiol A-Chem 356:364
43. Kang S-F, Liao C-H, Po S-T (2000) Chemosphere 41:1287
44. Olya ME, Aleboyeh H, Aleboyeh A (2012) J Adv Oxid Technol 5:41
45. Srithep S, Phattarapattamawong S (2017) Chemosphere 176:25
46. Oppenländer T (2007) Photochemical purification of water and air: advanced oxidation processes (AOPs)-principles, reaction mechanisms, reactor concepts, John Wiley & Sons, New York
47. Chan C, Tao S, Dawson R, Wong P (2004) Environ Pollut 131:45
48. Turchi CS, Ollis DF (1990) J Catal 122:178
49. Cornish BJ, Lawton LA, Robertson PK (2000) Appl Catal B-Environ 25:59
50. Czaplicka M, Hazard J (2006) Mater 134:45
51. Dionysiou DD, Suidan MT, Baudin I, Laîné J-M (2004) Appl Catal B-Environ 50:259
52. Łęcki T, Zarębska K, Sobczak K, Skompska M (2019) Appl Surf Sci 470:991
53. Galindo C, Kalt A (1999) Dyes Pigment 42:199
54. Wakimoto R, Kitamura T, Ito F, Usami H, Moriwaki H (2015) Appl Catal B Environ 166:544
55. Kato A, Cvetanović RJ (1968) Can J Chem 46:235
56. Eyasu A, Yadav O, Bachheti R (2013) Int J Chem Tech Res 5:1452
57. Gupta NK, Ghafari Y, Kim S, Bae J, Kim KS, Saifuddin M (2020) Sci Rep 10:1
58. Bouchaaba H, Bellal B, Maachi R, Trari M, Nasrallah N, Mellah A (2016) J Taiwan Instit Chem Eng 58:310
59. Saeed K, Khan I (2017) Turkish J Chem 41:391
60. Sharma O, Sharma MK (2013) Int J Chem Tech Res 5:1615
61. Fu S, Niu H, Tao Z, Song J, Mao C, Zhang S, Chen C, Wang D (2013) J Alloy Comp 576:5